Title

Crystallinity of Double-Stranded RNA-Antimicrobial Peptide Complexes Modulates Toll-Like Receptor 3-Mediated Inflammation

Journal

ACS Nano, 11(12)

ISSN

1936-0851

Authors

Lee, Ernest Y
Takahashi, Toshiya
Curk, Tine
et al.

Publication Date

2017-12-26

DOI

10.1021/acsnano.7b05234

Peer reviewed

HHS Public Access

Author manuscript

ACS Nano. Author manuscript; available in PMC 2018 May 06.

Published in final edited form as:

ACS Nano. 2017 December 26; 11(12): 12145–12155. doi:10.1021/acsnano.7b05234.

Crystallinity of Double-Stranded RNA-Antimicrobial Peptide Complexes Modulates Toll-Like Receptor 3-Mediated Inflammation

Ernest Y. Lee[1], **Toshiya Takahashi**[2], **Tine Curk**[3], **Jure Dobnikar**[3,4,5,*], **Richard L. Gallo**[2,*], and **Gerard C. L. Wong**[1,*]

[1]Department of Bioengineering, University of California, Los Angeles, Los Angeles, CA 90095, United States

[2]Department of Dermatology, University of California, San Diego, La Jolla, CA 92093, United States

[3]Beijing National Laboratory for Condensed Matter Physics & CAS Key Laboratory of Soft Matter Physics, Institute of Physics, Chinese Academy of Sciences, Beijing 100190, China

[4]Department of Chemistry, University of Cambridge, Cambridge, UK

[5]School of Physical Sciences, University of Chinese Academy of Sciences, Beijing 100049, China

Abstract

Double-stranded RNA (dsRNA) induces production of pro-inflammatory cytokines in normal human epidermal keratinocytes (NHEK) by specific binding to endosomal Toll-like receptor-3 (TLR3). Recently, it has been shown that hyperactivation of TLR3 in psoriatic keratinocytes by dsRNA can occur in the presence of human antimicrobial peptide (AMP) LL37. Here, we combine synchrotron X-ray scattering, microscopy, computer simulations, and measurements of NHEK cytokine production to elucidate a previously unanticipated form of specific molecular pattern recognition. LL37 and similar α-helical AMPs can form proinflammatory nanocrystalline complexes with dsRNA that are recognized by TLR3 differently than dsRNA alone. dsRNA complexes that activate IL-6 production in NHEK and those that do not are both able to enter cells and colocalize with TLR3. However, the crystallinity of these AMP-dsRNA complexes, specifically the geometric spacing between parallel dsRNA and the repeat number of ordered dsRNA, strongly influence the level of TLR3 activation. Crystalline complexes that present dsRNA at a spacing that matches with the steric size of TLR3 can recruit and engage multiple TLR3 receptors, driving receptor clustering and immune amplification, whereas crystalline complexes that exhibit poor steric matching do not. Reverse-transcription quantitative PCR (RTqPCR) of IL-6 during siRNA knockdown of TLR3 confirms that cytokine production is due to TLR3: High levels of IL-6 transcription are observed for sterically-matched complexes without TLR3 knockdown, whereas such activity is abrogated with TLR3 knockdown.

*To whom correspondence should be addressed: Gerard C.L. Wong, Department of Bioengineering, University of California, Los Angeles, 4121 Engineering V UCLA Los Angeles, CA 90095. Tel: (310) 794-7684 gclwong@seas.ucla.edu, Richard L. Gallo, Department of Dermatology, University of California, San Diego, 3350 La Jolla Village Drive, San Diego, CA 92161. rgallo@ucsd.edu, Jure Dobnikar, Institute of Physics, Chinese Academy of Sciences, Beijing, China. jd489@cam.ac.uk.

Keywords

dsRNA; toll-like receptors; psoriasis; antimicrobial peptides; innate immunity

TLR3 recognition of dsRNA is a fundamental example of molecular recognition.[1] Binding of viral dsRNA to TLR3 in endosomes triggers downstream NF-kB activation and production of pro-inflammatory cytokines.[2,3] Recently, non-coding host-derived dsRNA has also been shown to break immune tolerance and activate TLR3, but these dsRNAs require presence of the antimicrobial peptide (AMP) LL37.[4] In psoriasis, self-dsRNA can complex with LL37, access endosomes, potently activate TLR3 in keratinocytes[5–8] and amplify production of the pro-inflammatory cytokines IL-6 and IFN-β,[9] thereby exacerbating disease.[10] A variety of RNA-binding proteins,[11,12] AMPs,[13] cell-penetrating peptides,[14] cationic lipids,[15] and synthetic polymers[16] have also been reported to bind to dsRNA. However, there is no general criterion to determine which of these self-assembled dsRNA complexes induce immune responses and which do not. A common hypothesis explaining the ability of complexed nucleic acids to activate endosomal immune receptors is that formation of aggregates confers increased efficiency of endosomal access and protection from nuclease degradation.[17] Although this model can explain why self-antigens can activate TLRs, it does not explain why some complexes are pro-inflammatory while others are non-inflammatory. Recent results on activation of TLR9 by dsDNA complexes suggest that cooperativity of ligand binding may be important,[18] but it is not clear whether these results are generalizable. At present, the mechanism for TLR3 activation by polycation-dsRNA complexes is not well understood.

It is not surprising that anionic dsRNA and cationic molecules can form electrostatic complexes, which have been studied extensively.[19–25] Perhaps a little more surprising is the observation that polycation-dsRNA complexes that activate IL-6 production and those that do not are both able to enter cells efficiently and colocalize with endosomal TLR3 in normal human epidermal keratinocytes (NHEK), which shows that the ability to access endosomal compartments, a necessary condition of activation, is not the only determinant for strong immune activation. What is unanticipated is the discovery against expectation that TLR3 immune activation depends strongly on the recognition of crystallinity in dsRNA-AMP complexes, and metrics of crystalline order can drive immune outcomes. The two major criteria defining TLR3 activation and amplification are 1) the inter-dsRNA spacing between parallel dsRNA ligands within the dsRNA complex, and 2) the average size (the average number of unit cells) of ordered crystalline domains within dsRNA complexes. These criteria, the lattice constant and the domain size, correspond to two fundamental measures of crystallinity. We rationalize this behavior using a coarse-grained computational model and show that TLR3 binding to dsRNA is optimized when the inter-dsRNA spacings are in an optimum range: Crystalline complexes that present dsRNA at a spacing well-matched with the TLR3 steric size can recruit and engage multiple TLR3 receptors, effectively driving receptor clustering and immune amplification, whereas complexes that exhibit poor steric matching do not. Our observations are consistent with a conceptual framework in which activation levels are modulated by different inter-RNA spacings and by different crystalline RNA domain sizes in AMP-dsRNA complexes. Importantly, reverse-transcription

quantitative PCR (RTqPCR) of IL-6 during siRNA knockdown of TLR3 confirms that observed cytokine production is due to TLR3: High levels of IL-6 transcription are observed for sterically-matched complexes without knockdown, whereas abrogation of such activity is observed for these complexes with TLR3 knockdown. Recent work on TLR9 has shown that complexes between dsDNA and polycations at optimal inter-DNA spacings (such as LL37) can lead to a drastic increase of interferon-α secretion by plasmacytoid dendritic cells, whereas those at mismatched spacings do not.[18] Taken together with the evidence adduced here, these cognate observations suggest that AMP-induced ligand clustering and crystalline ordering can lead to an unexpected channel of pattern recognition and amplification for TLR responses, and a potentially general mode of AMP immunomodulatory function.

Results and Discussion

IL-6 production in keratinocytes through TLR3 activation depends on the inter-dsRNA spacing within self-assembled polycation-dsRNA electrostatic complexes

The structural basis of dsRNA binding by TLR3 has been demonstrated *via* X-ray crystallography[26] (Figure 1A). dsRNA can bind electrostatically *via* the anionic phosphate backbone to cationic portions of TLR3 dimers. Since complexes of dsRNA and various cationic molecules can lead to high levels of immune activation,[27] we investigate their structures. The structures of dsRNA complexes with immunologically relevant polycations, many of which are amphiphilic and impart an additional principle of self-assembly, are largely unknown. To assess the relationship between keratinocyte activation and these peptide-dsRNA complexes, we characterized 15 polycation-dsRNA structures with SAXS and correlated these structures with their ability to activate NHEK cells. Consistent with the behavior of other electrostatic complexes composed of nucleic acids,[28] the observed structures do not depend strongly on the global concentration of these complexes. The structures of these complexes, however, can in principle change with the composition of the complex. To mitigate this uncertainty, we solved each individual structure at three or more different polycation-to-dsRNA molar ratios on both sides of the isoelectric point, the stoichiometry at which the negative charge of the dsRNA is compensated by the positive charge of the polycation (typically obtained from the polycation to dsRNA charge ratio, P/RNA = 1/4, 1/2, 1/1, 2/1, 4/1). This library of over 50 solved structures, which covers a large range of physiologically relevant scenarios, is organized into a “phase diagram” for each type of complex. We find that the self-assembled structures of these dsRNA complexes are remarkably conserved for a broad range of stoichiometry with minor exceptions. Typical structures are dsRNA columnar phases with different in-plane symmetries (square lattices, hexagonal lattices, disordered lattices), and with different spacings between dsRNA (center-to-center distances between dsRNA). From each structure, we measure the inter-dsRNA spacing a, the linear domain size L (and the repeat number m) (Table S1). Details are found in the Supplementary Information.

To assess the level of immune activation induced by each complex, IL-6 protein production is measured as a quantitative readout for NHEK activation using ELISA (Table S1). IL-6 is one of several primary cytokines implicated in the pathogenesis of psoriasis, and frequently serves as a reporter cytokine for TLR-mediated activation of inflammation through NF-kB.

While dendritic cells and T cells are important cell types in the pathogenesis of psoriasis, keratinocytes have been clearly implicated as key participants in the immune response to nucleic acids, including acting as a main source of type 1 interferon production.[29] The data shows that some dsRNA complexes strongly amplify TLR3 activation while others do not. To investigate the origin of this difference, we compare the measured level of IL-6 production with the inter-dsRNA spacing and unit cell repeat number of each complex for each set of stoichiometric conditions in our phase diagram. We find that there is a strong relationship between the structure of polycation-dsRNA immune complexes and their ability to amplify IL-6 production. Specifically, immune complexes with inter-dsRNA spacings much smaller than TLR3 do not activate strongly (Figure 1B), while complexes with inter-dsRNA spacings roughly commensurate with the size of TLR3 maximize activation (Figure 1C). We have chosen to illustrate these differences by highlighting four prototypical examples of polycation-dsRNA complexes with varying structures. HIV-TAT is a well-characterized cell-penetrating peptide that has been explored as a nucleic acid transfection reagent, and is known to have strong endosomal access.[30,31] Buforin is an antimicrobial peptide obtained from a histone fragment that is known to penetrate cell membranes and bind to nucleic acids.[32,33] Spermine is an endogenous polyamine known to be biologically important in the folding and binding of nucleic acids to their targets,[34–36] and is a structural relative of many cationic polymers used for gene delivery applications. LL37 is a multifunctional endogenous innate immunity peptide that is implicated in the pathogenesis of autoimmune disease such as lupus and psoriasis.[17,37,38] It can also form pores in membranes, enable endosomal access, and has been reported to signal to the immune system *via* TLR9.[39]

From SAXS measurements, the TAT-dsRNA complex forms a close-packed 3D hexagonal columnar lattice with a first peak position at $q_{100} = 0.217$ Å^{-1} and higher order reflections at $q_{001} = 0.271$, $q_{110} = 0.384$, and $q_{200} = 0.441$ Å^{-1}, corresponding to an inter-dsRNA spacing of $a \sim 2.90$ nm, which is much smaller than the steric size of TLR3 (Figure 1B, 1D). In contrast, the structure of the buforin-dsRNA complex is an “open” 2D hexagonal columnar lattice with a first peak position at $q_{10} = 0.182$ Å^{-1} and higher order reflections at $q_{11} = 0.314$ Å^{-1}, $q_{20} = 0.362$ Å^{-1}, and $q_{21} = 0.482$ Å^{-1}, corresponding to a larger inter-dsRNA spacing of $a \sim 3.45$ nm that can accommodate the size of TLR3 (Figure 1C, 1D). dsRNA complexes based on TAT induce low levels of IL-6 even though TAT is known to exhibit pervasive endosomal access in a broad range of cells. In comparison, dsRNA complexes based on buforin exhibits high levels of IL-6 production, with the latter inducing an order of magnitude (~10×) more IL-6 production than TAT-dsRNA complexes (Figure 1E). SAXS measurements show that spermine-dsRNA complexes form tightly packed hexagonal columnar arrays, corresponding to an inter-dsRNA spacing of $a \sim 2.69$ nm (Figure 2A, 2B). In contrast, LL37-dsRNA complexes exhibited a single diffraction peak at $q_1 = 0.173$ Å^{-1} corresponding to an average inter-dsRNA spacing of 3.63 nm, consistent with an “open” disordered columnar complex (Figure 2A, 2C). Like buforin, LL37-dsRNA complexes induce high levels of IL-6 production from NHEK, consistent with prior experimental observations,[27] but spermine-dsRNA complexes, like TAT-dsRNA complexes, do not. Quantitatively, complexes based on LL37 induce ~5× more IL-6 from NHEK than those based on spermine. The disparity between IL-6 expression levels induced by LL37- and

buforin-dsRNA with those induced by TAT- and spermine-dsRNA complexes illustrate two distinct families of structures that differentially predict immune activation (Figure 1B, 1C, 2C). In fact, our immune activation data for the 15 different dsRNA complexes suggest that the measured inter-dsRNA spacings in these complexes correlate strongly with TLR3 activation (Figure 1E). Generally, we observed that complexes with first peak positions ~1.7–1.9 nm^{-1} strongly activated TLR3, while those outside this range had reduced abilities to activate TLR3. We note that although most complexes follow the trend line, a small subset of complexes appears to deviate slightly. This is not surprising given the complex nature of TLR activation: For example, it is possible that small quantitative differences in the degree of endosomal access between different types of dsRNA-peptide complexes can influence the level of the IL-6 response. In particular, from our previous SAXS experiments with model membranes, helical AMPs like LL37, CRAMP, and their mutants exhibit different levels of membrane curvature generating activity due to differences in charge, hydrophobicity, and amphipathicity,[40] which can alter their intake pathways and thereby TLR access. Differential degradation rates of these peptides in biological environments may also play a role in the observed variation. In fact, our characterization of the structures of a cohort of LL37 fragments bound to dsRNA mimics the distribution of LL37 degradation products likely present *in vivo*.[41,42]

The majority of the characterized polycation-dsRNA complexes did not exhibit significant changes in the first-peak positions across the wide range of tested peptide-to-dsRNA stoichiometric ratios (and by implication charge ratios), indicating that most of these structures are robust to changes in relative stoichiometry. Moreover, the LL37-dsRNA complex was found to be stable in human serum, which indicates that the self-assembly process is robust even in the presence of other proteins. Indeed, this is not unexpected on physics grounds: Electrostatic self-assembly at physiological conditions favors binding between components with equal and opposite surface charge densities due to the resultant maximal entropy gain of counterion release,[43] which is the case for dsRNA and LL37. However, a small subset of the tested peptide-dsRNA complexes (EF15 and LL34) exhibited a small shift in their first peak position from a lower to higher q as the peptide-to-dsRNA charge ratio increased from below the isoelectric point (P/RNA = 1/4, 1/2) to isoelectric (P/RNA = 1/1) and beyond (P/RNA = 2/1, 4/1). This behavior indicates that the structure of the complex is changing with stoichiometry. However, it is interesting to note that these data points also follow the basic trend line (Figure 1E)

Potential relationship between TLR3 activation and the inter-RNA spacing within dsRNA complexes

The potential structural criterion outlined above is an interesting finding, given that the prevailing paradigm of immune activation is that the spatial organization of dsRNA ligands is not expected to influence the magnitude of activation. To test the statistical significance of these trends, we construct a null hypothesis based on the assumption that there is no relationship between TLR3 activation (as measured by IL-6 secretion) and the inter-dsRNA spacing. The inter-dsRNA spacings (inversely proportional to first-peak position q) and the magnitude of TLR3 activation are assumed to be two random variables. That the present problem involves nonlinear correlations dictates that it is necessary to go beyond the usual

linear statistical methods. To this end, we used the recently developed metric distance correlation (R_{dCor})[44,45] to quantify the association between our paired variables without assuming any functional form of the correlation (*e.g.* fitting the data parametrically to a function). By definition, R_{dCor} takes on values between 0 and 1. $R_{dCor} = 0$ if and only if the variables are statistically independent, while $R_{dCor} = 1$ if strongly dependent. Using a Monte-Carlo simulation (N = 100,000 sampling iterations), we randomly sampled the experimental dataset of measured IL-6 production for polycation-dsRNA complexes with the null hypothesis that there is no correlation between the structure of the complexes and IL-6 activation. We find that the distance correlation between the inter-dsRNA spacing and TLR3 activation is $R_{dCor} = 0.371$ [0.327, 0.492] with P = 0.022 at a 95% significance level of $\alpha = 0.05$ (Figure S1A), indicating a likely relationship between TLR3 activation and inter-RNA spacing. To test this finding further, we also calculated the recently developed maximal information coefficient (MIC), which non-parametrically measures the strength of the non-linear association between paired variables.[46] Like dCor, MIC takes on values between 0 and 1. MIC values close to 0 indicate statistical independence while values near 1 indicate a strong functional relationship. Using a similar Monte-Carlo simulation (N = 100,000), we conducted a null-hypothesis significance test using MIC.[47] The MIC correlation between inter-dsRNA spacing and TLR3 activation was MIC = 0.652 [0.414, 0.894] with $P < 10^{-5}$ at a 95% significance level of $\alpha = 0.05$ (Figure S1B). Taken together, these two results suggest that the null hypothesis is highly unlikely, and that there is clearly a statistically significant nonlinear relationship between TLR3 activation and the inter-RNA spacings of self-assembled RNA complexes.

Cytokine-inducing polycation-dsRNA complexes activate NHEK *via* TLR3

From the data in Figure 1E, we observed that IL-6 amplifying and non-IL-6-amplifying molecules activate TLR3 to varying degrees. To assay whether polycation-dsRNA complexes indeed co-localize with and activate specifically through TLR3, we carried out fluorescence microscopy experiments and RTqPCR experiments with NHEK. We tested one IL-6 amplifying complex (LL37) and two non-amplifying complexes (TAT and spermine). From microscopy studies of prototypical examples of dsRNA-polycation complexes, we find that dsRNA complexes that amplify NHEK production of IL-6 and those that do not both enter cells and colocalize with TLR3 (Figure 3A). Interestingly, LL37-dsRNA, TAT-dsRNA, and spermine-dsRNA all enter NHEK cells and apparently bind to TLR3. However, only LL37-dsRNA complexes seem to amplify cytokine production, while the other complexes do not. These results suggest that internalization and access to immune cells, while clearly important to be sure, do not by themselves explain differences in levels of immune activation. Entry and binding to TLR3 is necessary but not sufficient for immune amplification. Rather, the inter-dsRNA spacing appears to play an important role also. To confirm that the cytokine production is indeed specifically due to TLR3, we conducted RTqPCR of IL-6 during siRNA knockdown of TLR3 in the presence and absence of the complexes. We observe high levels of IL-6 transcription for IL-6-amplifying LL37-dsRNA, Peptide 2-dsRNA, and buforin-dsRNA complexes without knockdown, and the abrogation of such activity with TLR3 knockdown, suggesting that activation of TLR3 by these complexes directly leads to cytokine production (Figure 3B) ($p^* < 0.05$ for dsRNA only, $p^{***} < 0.001$ for buforin-dsRNA, $p^{**} < 0.01$ for Peptide 2-dsRNA, $p^* < 0.05$ for LL37-dsRNA). To

confirm that the siTLR3 indeed knocked down TLR3 expression, we also measured TLR3 expression *via* RTqPCR (Figure 3C) ($p < 0.001$). Although it is generally recognized that siRNA knockdown is not always completely efficient, we observe significant knockdown of IL-6 transcription. We note that it is possible that some residual IL-6 production may be present due to endosomal escape and activation of the cytoplasmic MAVS signaling pathway by dsRNA complexes. In summary, IL-6 induction by polycation-dsRNA complexes are mediated at least in part by TLR3, and maximally-inducing complexes exhibit similar degrees of endosomal access as non-amplifying complexes.

Coarse-grained model of TLR3 binding to RNA bundles exhibits dependence on inter-dsRNA spacing and repeat number in agreement with experimental observations

To investigate TLR3 interactions with ordered dsRNA immune complexes, we developed a coarse-grained theoretical model, which aims to predict the fraction of ligand-bound, active TLR3 receptors $f_A(q, m)$ as a function of the crystallinity parameters $q = 2\pi/a$ (where a is the inter-dsRNA spacing) and m (repeat number of RNA in the complex) (Figure 4A). Experimentally, the repeat number m is calculated from the linear domain size L (see Supplementary Information). The dsRNA complex/TLR3 system is cognate to the dsDNA complex/TLR9 system, which we have previously engaged.[18,48] Based on crystallography data, TLR3[26] has a larger opening angle compared to TLR9.[49] Therefore, we predict that the optimal lattice spacing resulting in maximal TLR3 activation will be larger for RNA-peptide complexes compared to DNA-peptide complexes. That dsRNA complexes exhibit different domain sizes affords us the opportunity to explicitly take into consideration the effect of varying the repeat number of polycation-dsRNA complexes on TLR3 activation, in addition to the inter-dsRNA spacing. We also take into account the variable strength of the TLR3-dsRNA backbone interactions and explicitly include the density of TLR3 in the endosome and average dsRNA length. To do this, we use a Langmuir-like approach and assume that there are k possible binding sites for TLR3 receptors on each dsRNA cluster (*i.e.* k is the maximum number of TLR3 receptors that can bind to each peptide-dsRNA cluster), with all binding sites identical and independent. The number k is determined by the repeat number m and the individual dsRNA length. Here, the TLR3 receptor molecules interact only through the hard-core excluded volume interaction forbidding their overlap. The total number of bound TLR3 is given by a Langmuir isotherm $n_B = k\frac{(1-f_A)e^{-\varepsilon(a)/k_BT}}{1+(1-f_A)e^{-\varepsilon(a)/k_BT}}$.

The single TLR3 binding free energy $\varepsilon(a) = \Delta G + \mu^{TLR} + 2U(a)$ includes 3 terms. The backbone electrostatic interaction $U(a)$ varies with the lattice spacing a due to the presence of adjacent anionic RNA rods in the nanocrystalline cluster.[18] $U(a)$ is characterized by two parameters: B, the magnitude of the screened electrostatic interactions, and σ, the steric length scale associated to the size of TLR3 receptors. The functional form of U and the realistic values of the parameters are given in the Supplementary Information (Eq. SI 5). The first two terms in thje expression for the binding free energy, $\varepsilon^* = \Delta G + \mu^{TLR}$ do not depend on crystallinity and are treated as a constant parameter. Here ΔG is the "pure" TLR3-dsRNA Gibbs interaction free energy and μ^{TLR} the activation-independent part of the chemical potential of TLR3 in the endosomal membrane. The part of the chemical potential that

depends on the fraction f_A of activated (bound) receptors is included explicitly in the theory and results in the prefactors $(1 - f_A)$ in the above expression n_B for the number of bound TLR3. Note that in our model we explicitly consider receptor depletion: more bound TLR3 leads to fewer available TLR3, increasing the cost of recruitment. The fraction of all active receptors is $f_A = \frac{n_b N_c}{N^{tot}}$, with N_c the average number of clusters on the membrane and N^{tot} the total number of TLR3 receptors. Assuming equilibrium between clusters in solution and those adsorbed to a membrane, we can determine f_A using a self-consistent relationship from multivalent adsorption theory[18,50,51] (see SI Eqn 3).

In Figure 4B, we present a contour plot of the fraction of active TLR3 receptors f_A (and predicted immune activation profile) as a function of the first peak position q and the repeat number m (a contour plot showing the fraction of active TLR3 receptors as function of the interaction strength ε and repeat number m is found in Figure S2). We assume that f_A is a good proxy for TLR3 activation and IL-6 production, with a larger fraction of active receptors correlating with increased immune activation and cytokine secretion. Using the approximate model here, a strong dependence on the inter-dsRNA spacing is observed. Moreover, a dependence on the repeat number m is also clearly observed. At larger m, dsRNA complexes with a broader range of inter-dsRNA spacings can maximally activate TLR3, while at smaller m, a narrower range of spacing is allowed (Figure S3A). At an inter-dsRNA spacing that is highly commensurate (well-matched) with the steric size of TLR3, even relatively small ligand clusters with a low number of repeats m can significantly activate due to strong multivalency and resultant "superselective" effects.[50,51] Interestingly, at spacings slightly larger than the steric size, a large m can compensate for reduced effective binding energy between sterically-mismatched dsRNA ligands and TLR3 (Figure S3B), while at spacings smaller than the steric size this is not possible. These observations suggest that the elastic response of dsRNA-AMP nanocrystals to deformations can influence binding to TLR3 and thereby immune activation. For spacings much larger or smaller than the TLR3 size, we observe a sharp drop in number of bound TLR3 ($q > 2.0$ nm^{-1}). This trend is reflected in the experimental data: polycation-dsRNA clusters with small inter-dsDRNA spacings ($q > 2.0$ nm^{-1}) like HIV-TAT and spermine cannot potentiate TLR3 activation despite having a large domain size ($L \sim 17$ nm for both TAT and spermine). In contrast, buforin-dsRNA and LL37-dsRNA complexes have quite different domain sizes and number of repeats, but since both have ideal inter-dsRNA spacing, they both activate NHEK. The buforin complex has a larger repeat number m than the LL37 complex (Table S1), explaining the higher relative levels of IL-6 induction by buforin-dsRNA. Indeed, in Figure 4C, we show that the fraction of active TLR3 receptors f_A can be predicted from both the experimentally measured inter-dsRNA spacing and the repeat number m, and that there is good correspondence between the model (black) and experimentally measured IL-6 secretion (red, data reproduced from Figure 1E).

To understand how the fraction of activated TLR3 depends on the crystallinity of TLR3-AMP complexes, we conducted coarse-grained Grand canonical Monte-Carlo simulations on TLR3-dsRNA binding (details in Supplementary Information). The fraction of bound and activated TLR3 receptors f_A for multiple dsRNA-AMP complexes with varying inter-dsRNA

spacings a is calculated. In Figure 4D, simulation results for f_A vs $q = 2\pi/a$ are shown for cluster size $m = 4$. For an interaction energy of $\varepsilon^* = 3\ k_B T$, the fraction of active TLR3 is maximized for complexes with 1st order diffraction peaks near $q \sim 1.85\ nm^{-1}$, which agrees well with experiment. A simulation snapshot of the dsRNA-TLR3 system near this corresponding optimal a spacing (such as for LL37-dsRNA) is shown in Figure S4. For interaction energies of $\varepsilon^* = 4\ k_B T$ and $5\ k_B T$, the dependence of f_A on q is weaker, but activation is still maximized at a comparable inter-dsRNA spacing. Note that the optimal spacing observed here is slightly larger than that of the cognate TLR9 system, due to geometric differences in size between TLR3 and TLR9. Comparison to experiment (Figure 1E, 4C) indicates that an interaction energy of $\varepsilon^* = 3\ k_B T$ is appropriate. The results also show that TLR3 binding and activation are more permissive for complexes with spacings that are sterically larger than the receptor than complexes with spacings that are smaller, in qualitative agreement with both the theoretical model and experiments.

The theoretical and simulation models address two limiting regimes of behavior: The former calculates TLR3 activation in a system where the total activation is limited by the number of available TLR3, whereas the latter assumes that the number of available TLR3 is large and the limiting constraint is the concentration of RNA-peptide complexes. The fact that we observe consistent behavior in these two limiting cases of TLR3 saturation and excess gives us confidence that we can address the basic aspects of the observed phenomenon with these simple models. Taken together, the dependence on the inter-dsRNA spacing, on the domain size and repeat number of dsRNA ordering, the residual ability of complexes with sterically larger dsRNA spacings to activate (especially with larger numbers of unit cells), and the inability of complexes with sterically smaller dsRNA spacings to activate, strongly suggest that the crystallinity of the dsRNA complex can structurally influence TLR3 activation significantly (Figure 5).

Conclusions and Prospects

In summary, we demonstrate that the presentation of ordered lattices of dsRNA leads to amplification of TLR3 mediated IL-6 cytokine production in NEHKs. That it was recently shown that the presentation of ordered crystalline lattices of dsDNA leads to amplification of TLR9 mediated interferon-α secretion in plasmacytoid dendritic cells suggests that these may not be unrelated phenomena[18,52,53] (It will be interesting to examine whether any other proinflammatory cytokines or cell types also exhibit similar amplification mechanisms.) These results suggest a general picture in which immune signaling can be strongly influenced by AMP-immune ligand interactions. The resultant “ligand clustering” can in principle drive receptor clustering. The data here suggest that cationic proteins, peptides, or other cationic agents less than ~0.5 nm in size or much greater than ~3 nm in size do not significantly activate TLR3, since steric constraints will prevent the crystalline dsRNA rods from effectively recruiting TLR3. It is evident that immune modulation is complex and multifactorial. Quantitative differences in the degree of endosomal access between different types of dsRNA-peptide complexes can influence the level of TLR3 response in a manner independent of the nanocrystalline multivalent binding model. What is also equally clear is that not only can AMPs organize dsRNA into nanocrystalline structures recognizable by

TLR3, the quantitative degree of immune activation is strongly influenced by crystalline parameters such as the inter-ligand spacing and the domain size of the ordering.

Materials and Methods

Preparation of self-assembled polycation-dsRNA complexes

Lyophilized cationic peptides LL37 (LLGDFFRKSKEKIGKEFKRIVQRIKDFLRNLVPRTES), buforin (TRSSRAGLQFPVGRVHRLLRK), CRAMP (GLLRKGGEKIGEKLKKIGQKIKNFFQKLVPQPEQ), and HIV-TAT (47–57, YGRKKRRQRRR) were purchased from Anaspec or Genemed Synthesis Inc. (≥95% purity by HPLC). The following cationic peptides were also custom synthesized (LifeTein, ≥95% purity by HPLC): GD35 (GDFFRKSKEKIGKEFKRIVQRIKDFLRNLVPRTES), LL34 (LLGDFFRKSKEKIGKEFKRIVQRIKDFLRNLVPR), LL30 (LLGDFFRKSKEKIGKEFKRIVQRIKDFLRN), KR20 (KRIVQRIKDFLRNLVPRTES), EF15 (EFKRIVQRIKDFLRN), Peptide 1, and Peptide 2. Other polycationic agents used include human lysozyme, polylysine (MW ~ 70,000), spermine, and protamine sulfate (Sigma Aldrich). All cationic agents were dissolved in nuclease-free water (Ambion) to 10 mg/mL. For SAXS and cell experiments, poly(I:C) (high molecular weight) and poly(A:U) (Invivogen) were directly resuspended in physiological buffer (100 mM NaCl + 10 mM HEPES, pH 7.4) to 5 mg/mL. Polycation-dsRNA complexes were formed by incubating the peptide with dsRNA (1–5 mg/mL for SAXS experiments, 10–20 μg/mL for cell experiments) at specific peptide-to-RNA charge ratios (P/RNA = 1/4, 1/2, 1/1, 2/1, 4/1). For a specific cationic reagent, the same charge ratios were used in both SAXS and cell experiments.

SAXS Experiments and Data Analysis

We mapped out the structural phase diagrams of peptide-dsRNA complexes by incubating peptides (10 mg/mL) with dsRNA (5 mg/mL) at specific charge ratios in microcentrifuge tubes as described above. After thorough mixing and centrifugation, precipitated complexes are hermetically sealed in 1.5 mm quartz capillaries (Hilgenberg GmbH, Mark-tubes). SAXS experiments were performed at Stanford Synchrotron Radiation Lightsource (SSRL, Beamline 4-2) using monochromatic X-rays with an energy of 9 keV. A Rayonix MX225-HE detector (pixel size 73.2 μm) was used to measure the scattered radiation. Independent identical samples were prepared and measured over multiple timepoints to ensure consistency. 2D powder diffraction patterns were integrated using the Nika 1.74[54] package for Igor Pro 6.37 and FIT2D[55]. SAXS data were analyzed by plotting integrated scattering intensity against the momentum transfer q using Mathematica. Peak positions were measured by fitting diffraction peaks to a Lorentzian. Structures of complexes were solved by calculating ratios between the q-positions of all measured peaks and comparing them with the permitted reflections for known liquid-crystalline phases. The lattice parameter(s) of each phase were calculated by linear regression through points corresponding to measured and theoretical peaks. The lattice parameter a indicates the inter-dsRNA spacing between RNA columns. For each complex, the inter-dsRNA spacing a is estimated from the first peak position by the formula $a = 2\pi/q_1$.

To determine the phase and lattice parameters for each nanocrystalline complex, we measure the q peak positions and relate them to the Miller indices for powdered averaged phases. $q_{hk} = \frac{2\pi}{a}\sqrt{h^2 + k^2}$ for square columnar lattices, $q_{hk} = \frac{2\pi}{a}\sqrt{\frac{4}{3}(h^2 + k^2 + hk)}$ for hexagonal columnar lattices, and $q_1 = \frac{2\pi}{a}$ for disordered columnar lattices. Square and hexagonal lattices were assigned based on fitting the measured q positions to the above equations. Typical square lattices will have reflections at q_{10} and q_{11} with a ratio of 1:√2. In contrast, typical hexagonal lattices will have reflections at q_{10}, q_{11}, and q_{20} with a ratio of 1:√3:2. Procedures to assign these liquid-crystalline phases are similar to those found here.[23]

In addition to quantifying the lattice parameters and inter-dsRNA spacings in each complex, we also measured average domain size L of each complex. From that value, we extracted the number of repeat units m in each complex. To obtain the domain size, we approximated the structure factor peaks as squared-Lorentzians. Comparing Gaussian and squared-Lorentzian lineshapes, the Lorentzian lineshape yielded the best fit for all of the complexes. The form of the equation used for the fit was

$$S(q) = \frac{w^3}{4\pi\left(|q - q_0|^2 + \left(\frac{w}{2}\right)^2\right)^2}$$

where q_0 is the location of the peak and w is the peak width.[18] The experimental SAXS data was background subtracted, and the first peak for each complex was fitted using non-linear least square regression in Mathematica. The extracted value for peak width w can be related to the average linear domain size L using Warren's approximation.[56] For the squared-Lorentzian lineshape, the domain size is related to w *via* the equation.[57]

$$L = \frac{(8\pi)^{\frac{1}{2}}}{\frac{w}{2}}$$

We assume that a typical bundle has an area proportional to L^2. To calculate the number of repeat units in each complex m, we estimated this by dividing the linear domain size L by the measured inter-dsRNA spacings a ($m = L/a$). The resulting values for L and m for each liquid-crystalline complex are reported in Table S1.

Reverse transcription-quantitative PCR (RTqPCR) analyses

Control siRNA and TLR3 siRNA were purchased from Dharmacon. During each keratinocyte stimulation, 5 nM of each siRNA was electroporated into NHEKs as described previously.[58] Total cellular RNA was extracted using the PureLink RNA isolation kit and RNA was reverse transcribed to cDNA using iScript cDNA synthesis kit (Bio-rad). Quantitative, real-time PCR was performed on the CFX96 real time system (Biorad) using TaqMan® Gene Expression Master Mix. The expression of GAPDH gene was used as a house keeping gene to normalize data in human cells. Specific primer sequences are shown in Table S2 in the Supplementary Information.

Keratinocyte Stimulation Experiments

Primary neonatal human epidermal keratinocytes (NHEKs) were purchased from Invitrogen. NHEKs were grown in serum free EpiLife medium supplemented with 0.06 mM $CaCl_2$, EpiLife Defined growth supplements (EDGS) (Invitrogen) and antibiotics, and passage 4–6 cells were used for experiment. Cells at 60%–80% confluence were starved overnight without EDGS prior to treatment. NHEKs were treated with polycationic agent/peptide (10 ug/mL) or vehicle control mixed with poly(I:C) (0.3 ug/mL) for 6 hrs (RTqPCR) and 18 hrs (ELISA). IL-6 protein volume using supernatant for NHEKs after indicated stimulation were measured by human IL-6 ELISA kit (R&D systems, Minneapolis, MN) per manufacturer's protocol. All stimulation experiments were done in triplicate. IL-6 release for each polycation-dsRNA complex was normalized relative to control stimulation and reported in Table S1.

NHEK Immunofluorostaining Experiments

NHEKs were grown on 8-well chamber slides (Thermo Fisher Scientific, Waltham, MA, USA). NHEKs were stimulated with biotinylated poly(I:C) (Invivogen, San Diego, CA, USA) with LL37 (Genemed Synthesis), HIV-TAT, or Spermine for 4 hr. Then NHEK were fixed in 4% PFA for 10 mins prior to immunofluorescence staining. Fixed and permeabilized cells were incubated with anti-TLR3 antibody (ab137722, abcam, Cambridge, MA, USA) followed by streptavidin-conjugated AlexaFluor 488 (Thermo Fisher Scientific) and 576-coupled anti-rabbit secondary antibody (Thermo Fisher Scientific). Nuclei were counterstained with DAPI. All images were taken with an Olympus BX41 microscope.

Statistical Analyses

Bootstrapping calculations to compute confidence intervals and P-values were done using the distance correlation function in the 'energy' package in R. MIC bootstrapping calculations were done using the 'minerva' package in R. We tested the relationship between the inter-dsRNA spacing and cytokine production by conducting a null hypothesis significance test with a significance level of $\alpha = 0.05$. Analysis of RTqPCR siRNA knockdown data was done in Mathematica using pairwise two-tailed t-tests with a significance level of $\alpha = 0.05$.

Supplementary Material

Refer to Web version on PubMed Central for supplementary material.

Acknowledgments

E.Y.L. acknowledges support from the T32 Systems and Integrative Biology Training Program (T32GM008185), the T32 Medical Scientist Training Program, (T32GM008042), and the T32 Dermatology Scientist Training Program (T32AR071307) at UCLA. R.L.G. acknowledges support from NIH R01AR064781, R01AI116576, and R01AI052453. G.C.L.W. acknowledges support from NIH 1R21AI122212. X-ray research was conducted at Stanford Synchrotron Radiation Lightsource, SLAC National Laboratory, supported by the US DOE Office of Basic Energy Sciences under Contract No. DE-AC02-76SF00515.

References

1. Uematsu S, Akira S. Toll-Like Receptors (TLRs) and Their Ligands. Handb Exp Pharmacol. 2008; 183:1–20.
2. Alexopoulou L, Holt AC, Medzhitov R, Flavell RA. Recognition of Double-Stranded RNA and Activation of NF-kappaB by Toll-Like Receptor 3. Nature. 2001; 413:732–738. [PubMed: 11607032]
3. Murphy, K. Janeway's Immunobiology. Garland Pub; 2014.
4. Herrath, von MG, Bot A. Immune Responsiveness, Tolerance and dsRNA: Implications for Traditional Paradigms. Trends in Immunology. 2003; 24:289–292. [PubMed: 12810099]
5. Nelson AM, Reddy SK, Ratliff TS, Hossain MZ, Katseff AS, Zhu AS, Chang E, Resnik SR, Page C, Kim D, et al. dsRNA Released by Tissue Damage Activates TLR3 to Drive Skin Regeneration. Cell Stem Cell. 2015; 17:139–151. [PubMed: 26253200]
6. Zhang L-J, Gallo RL. Antimicrobial Peptides. Curr. Biol. 2016; 26:R14–R19. [PubMed: 26766224]
7. Miller LS. Toll-Like Receptors in Skin. Adv Dermatol. 2008; 24:71–87. [PubMed: 19256306]
8. Chen X, Takai T, Xie Y, Niyonsaba F, Okumura K, Ogawa H. Human Antimicrobial Peptide LL-37 Modulates Proinflammatory Responses Induced by Cytokine Milieus and Double-Stranded RNA in Human Keratinocytes. Biochem. Biophys. Res. Commun. 2013; 433:532–537. [PubMed: 23524263]
9. Grossman RM, Krueger J, Yourish D, Granellipiperno A, Murphy DP, May LT, Kupper TS, Sehgal PB, Gottlieb AB. Interleukin-6 Is Expressed in High-Levels in Psoriatic Skin and Stimulates Proliferation of Cultured Human Keratinocytes. Proc. Natl. Acad. Sci. U.S. A. 1989; 86:6367–6371. [PubMed: 2474833]
10. Goodman WA, Levine AD, Massari JV, Sugiyama H, McCormick TS, Cooper KD. IL-6 Signaling in Psoriasis Prevents Immune Suppression by Regulatory T Cells. 2009; 183:3170–3176.
11. Yang Y, Wang S-Y, Huang Z-F, Zou H-M, Yan B-R, Luo W-W, Wang Y-Y. The RNA-Binding Protein Mex3B Is a Coreceptor of Toll-Like Receptor 3 in Innate Antiviral Response. Cell Res. 2016; 26:288–303. [PubMed: 26823206]
12. Lai Y, Yi G, Chen A, Bhardwaj K, Tragesser BJ, Valverde Rodrigo A, Zlotnick A, Mukhopadhyay S, Ranjith-Kumar CT, Kao CC. Viral Double-Strand RNA-Binding Proteins Can Enhance Innate Immune Signaling by Toll-Like Receptor 3. PLoS ONE. 2011; 6:e25837. [PubMed: 22016778]
13. Ganguly D, Chamilos G, Lande R, Gregorio J, Meller S, Facchinetti V, Homey B, Barrat FJ, Zal T, Gilliet M. Self-RNA-Antimicrobial Peptide Complexes Activate Human Dendritic Cells Through TLR7 and TLR8. J. Exp. Med. 2009; 206:1983–1994. [PubMed: 19703986]
14. Endoh T, Ohtsuki T. Cellular siRNA Delivery Using Cell-Penetrating Peptides Modified for Endosomal Escape. Advanced Drug Delivery Reviews. 2009; 61:704–709. [PubMed: 19383521]
15. Bouxsein, Nathan F., McAllister, Christopher S., Ewert, Kai K., Charles E Samuel, A., Safinya, Cyrus R. Structure and Gene Silencing Activities of Monovalent and Pentavalent Cationic Lipid Vectors Complexed with siRNA†. Biochemistry. 2007; 46:4785–4792. [PubMed: 17391006]
16. Singha K, Namgung R, Kim WJ. Polymers in Small-Interfering RNA Delivery. Nucleic Acid Ther. 2011; 21:133–147. [PubMed: 21749290]
17. Gilliet M, Lande R. Antimicrobial Peptides and Self-DNA in Autoimmune Skin Inflammation. Curr. Opin. Immunol. 2008; 20:401–407. [PubMed: 18611439]
18. Schmidt NW, Jin F, Lande R, Curk T, Xian W, Lee C, Frasca L, Frenkel D, Dobnikar J, Gilliet M, et al. Liquid-Crystalline Ordering of Antimicrobial Peptide-DNA Complexes Controls TLR9 Activation. Nat Mater. 2015; 14:696–700. [PubMed: 26053762]
19. Wong GCL, Pollack L. Electrostatics of Strongly Charged Biological Polymers: Ion-Mediated Interactions and Self-Organization in Nucleic Acids and Proteins. Annu Rev Phys Chem. 2010; 61:171–189. [PubMed: 20055668]
20. Pollack L. SAXS Studies of Ion–Nucleic Acid Interactions. Annu. Rev. Biophys. 2011; 40:225–242. [PubMed: 21332357]
21. Livolant F, Leforestier A. Condensed Phases of DNA: Structures and Phase Transitions. Progress in Polymer Science. 1996; 21:1115–1164.

22. Sanders LK, Xian W, Guáqueta C, Strohman MJ, Vrasich CR, Luijten E, Wong GCL. Control of Electrostatic Interactions Between F-Actin and Genetically Modified Lysozyme in Aqueous Media. Proc. Natl. Acad. Sci. U. S. A. 2007; 104:15994–15999. [PubMed: 17911256]
23. DeRouchey J, Netz RR, Radler JO. Structural Investigations of DNA-Polycation Complexes. Eur. Phys. J. E. 2005; 16:17–28. [PubMed: 15688137]
24. Evans HM, Ahmad A, Ewert K, Pfohl T, Martin-Herranz A, Bruinsma RF, Safinya CR. Structural Polymorphism of DNA-Dendrimer Complexes. Phys. Rev. Lett. 2003; 91:075501. [PubMed: 12935030]
25. Rau DC, Parsegian VA. Direct Measurement of the Intermolecular Forces Between Counterion-Condensed DNA Double Helices. Evidence for Long Range Attractive Hydration Forces. Biophysj. 1992; 61:246–259.
26. Liu L, Botos I, Wang Y, Leonard JN, Shiloach J, Segal DM, Davies DR. Structural Basis of Toll-Like Receptor 3 Signaling with Double-Stranded RNA. Science. 2008; 320:379–381. [PubMed: 18420935]
27. Lai Y, Adhikarakunnathu S, Bhardwaj K, Ranjith-Kumar CT, Wen Y, Jordan JL, Wu LH, Dragnea B, Mateo LS, Kao CC. LL37 and Cationic Peptides Enhance TLR3 Signaling by Viral Double-Stranded RNAs. PLoS ONE. 2011; 6:e26632. [PubMed: 22039520]
28. Radler JO, Koltover I, Salditt T, Safinya CR. Structure of DNA-Cationic Liposome Complexes: DNA Intercalation in Multilamellar Membranes in Distinct Interhelical Packing Regimes. Science. 1997; 275:810–814. [PubMed: 9012343]
29. Zhang L-J, Sen GL, Ward NL, Johnston A, Chun K, Chen Y, Adase C, Sanford JA, Gao N, Chensee M, et al. Antimicrobial Peptide LL37 and MAVS Signaling Drive Interferon-B Production by Epidermal Keratinocytes During Skin Injury. Immunity. 2016; 45:119–130. [PubMed: 27438769]
30. Mishra A, Gordon VD, Yang L, Coridan R, Wong GCL. HIV TAT Forms Pores in Membranes by Inducing Saddle-Splay Curvature: Potential Role of Bidentate Hydrogen Bonding. Angew. Chem. Int. Ed. Engl. 2008; 47:2986–2989. [PubMed: 18338358]
31. Brooks H, Lebleu B, Vivès E. Tat Peptide-Mediated Cellular Delivery: Back to Basics. Advanced Drug Delivery Reviews. 2005; 57:559–577. [PubMed: 15722164]
32. Park CB, Kim HS, Kim SC. Mechanism of Action of the Antimicrobial Peptide Buforin II: Buforin II Kills Microorganisms by Penetrating the Cell Membrane and Inhibiting Cellular Functions. Biochem. Biophys. Res. Commun. 1998; 244:253–257. [PubMed: 9514864]
33. Park CB, Yi KS, Matsuzaki K, Kim MS, Kim SC. Structure-Activity Analysis of Buforin II, a Histone H2A-Derived Antimicrobial Peptide: the Proline Hinge Is Responsible for the Cell-Penetrating Ability of Buforin II. Proc. Natl. Acad. Sci. U. S. A. 2000; 97:8245–8250. [PubMed: 10890923]
34. Feuerstein BG, Williams LD, Basu HS, Marton LJ. Implications and Concepts of Polyamine-Nucleic Acid Interactions. J. Cell. Biochem. 1991; 46:37–47. [PubMed: 1874798]
35. Tabor CW, Tabor H. Polyamines. Annu. Rev. Biochem. 1984
36. Moinard C, Cynober L, de Bandt J. Polyamines: Metabolism and Implications in Human Diseases. Clinical Nutrition. 2005; 24:184–197. [PubMed: 15784477]
37. Lande R, Botti E, Jandus C, Dojcinovic D, Fanelli G, Conrad C, Chamilos G, Feldmeyer L, Marinari B, Chon S, et al. The Antimicrobial Peptide LL37 Is a T-Cell Autoantigen in Psoriasis. Nat Commun. 2014; 5:5621. [PubMed: 25470744]
38. Morizane S, Gallo RL. Antimicrobial Peptides in the Pathogenesis of Psoriasis. J Dermatol. 2012; 39:225–230. [PubMed: 22352846]
39. Lande R, Chamilos G, Ganguly D, Demaria O, Frasca L, Durr S, Conrad C, Schröder J, Gilliet M. Cationic Antimicrobial Peptides in Psoriatic Skin Cooperate to Break Innate Tolerance to Self-DNA. Eur. J. Immunol. 2015; 45:203–213. [PubMed: 25332209]
40. Lee EY, Fulan BM, Wong GCL, Ferguson AL. Mapping Membrane Activity in Undiscovered Peptide Sequence Space Using Machine Learning. Proc. Natl. Acad. Sci. U.S.A. 2016; 113:13588–13593. [PubMed: 27849600]

41. Yamasaki K, Schauber J, Coda A, Lin H, Dorschner RA, Schechter NM, Bonnart C, Descargues P, Hovnanian A, Gallo RL. Kallikrein-Mediated Proteolysis Regulates the Antimicrobial Effects of Cathelicidins in Skin. FASEB J. 2006; 20:2068–2080. [PubMed: 17012259]
42. Murakami M, Lopez-Garcia B, Braff M, Dorschner RA, Gallo RL. Postsecretory Processing Generates Multiple Cathelicidins for Enhanced Topical Antimicrobial Defense. J. Immunol. 2004; 172:3070–3077. [PubMed: 14978112]
43. Wong GCL. Electrostatics of Rigid Polyelectrolytes. Current Opinion in Colloid & Interface Science. 2006; 11:310–315.
44. Székely GJ, Rizzo ML, Bakirov NK. Measuring and Testing Dependence by Correlation of Distances. The Annals of Statistics. 2007; 35:2769–2794.
45. Székely GJ, Rizzo ML. Energy Statistics: a Class of Statistics Based on Distances. Journal of Statistical Planning and Inference. 2013; 143:1249–1272.
46. Reshef DN, Reshef YA, Finucane HK, Grossman SR, McVean G, Turnbaugh PJ, Lander ES, Mitzenmacher M, Sabeti PC. Detecting Novel Associations in Large Data Sets. Science. 2011; 334:1518–1524. [PubMed: 22174245]
47. Albanese D, Filosi M, Visintainer R, Riccadonna S, Jurman G, Furlanello C. Minerva and Minepy: a C Engine for the MINE Suite and Its R, Python and MATLAB Wrappers. Bioinformatics. 2013; 29:407–408. [PubMed: 23242262]
48. Lee EY, Lee CK, Schmidt NW, Jin F, Lande R, Curk T, Frenkel D, Dobnikar J, Gilliet M, Wong GCL. A Review of Immune Amplification *via* Ligand Clustering by Self-Assembled Liquid-Crystalline DNA Complexes. Adv Colloid Interface Sci. 2016; 232:17–24. [PubMed: 26956527]
49. Ohto U, Shibata T, Tanji H, Ishida H, Krayukhina E, Uchiyama S, Miyake K, Shimizu T. Structural Basis of CpG and Inhibitory DNA Recognition by Toll-Like Receptor 9. Nature. 2015; 520:702–705. [PubMed: 25686612]
50. Dubacheva GV, Curk T, Auzély-Velty R, Frenkel D, Richter RP. Designing Multivalent Probes for Tunable Superselective Targeting. Proc. Natl. Acad. Sci. U. S. A. 2015; 112:5579–5584. [PubMed: 25901321]
51. Dubacheva GV, Curk T, Mognetti BM, Auzély-Velty R, Frenkel D, Richter RP. Superselective Targeting Using Multivalent Polymers. J. Am. Chem. Soc. 2014; 136:1722–1725. [PubMed: 24400591]
52. Tursi SA, Lee EY, Medeiros NJ, Lee MH, Nicastro LK, Buttaro B, Gallucci S, Wilson RP, Wong GCL, Tükel Ç. Bacterial Amyloid Curli Acts as a Carrier for DNA to Elicit an Autoimmune Response *via* TLR2 and TLR9. PLoS Pathog. 2017; 13:e1006315. [PubMed: 28410407]
53. Lee EY, Takahashi T, Curk T, Dobnikar J, Gallo RL, Wong GCL. 070 Liquid Crystalline Ordering of Antimicrobial Peptide-RNA Complexes Controls TLR3 Activation. Journal of Investigative Dermatology. 2017; 137:S12.
54. Ilavsky J. Nika: Software for Two-Dimensional Data Reduction. J Appl Crystallogr. 2012; 45:324–328.
55. Hammersley AP. FIT2D: an Introduction and Overview. European Synchrotron Radiation Facility Internal Report: ESRF97HA02T. 1997
56. Warren BE. X-Ray Diffraction in Random Layer Lattices. Phys. Rev. 1941; 59:693–698.
57. Needleman DJ, Ojeda-Lopez MA, Raviv U, Miller HP, Wilson L, Safinya CR. Higher-Order Assembly of Microtubules by Counterions: From Hexagonal Bundles to Living Necklaces. Proc. Natl. Acad. Sci. U. S.A. 2004; 101:16099–16103. [PubMed: 15534220]
58. Borkowski AW, Park K, Uchida Y, Gallo RL. Activation of TLR3 in Keratinocytes Increases Expression of Genes Involved in Formation of the Epidermis, Lipid Accumulation, and Epidermal Organelles. J. Invest. Dermatol. 2013; 133:2031–2040. [PubMed: 23353987]

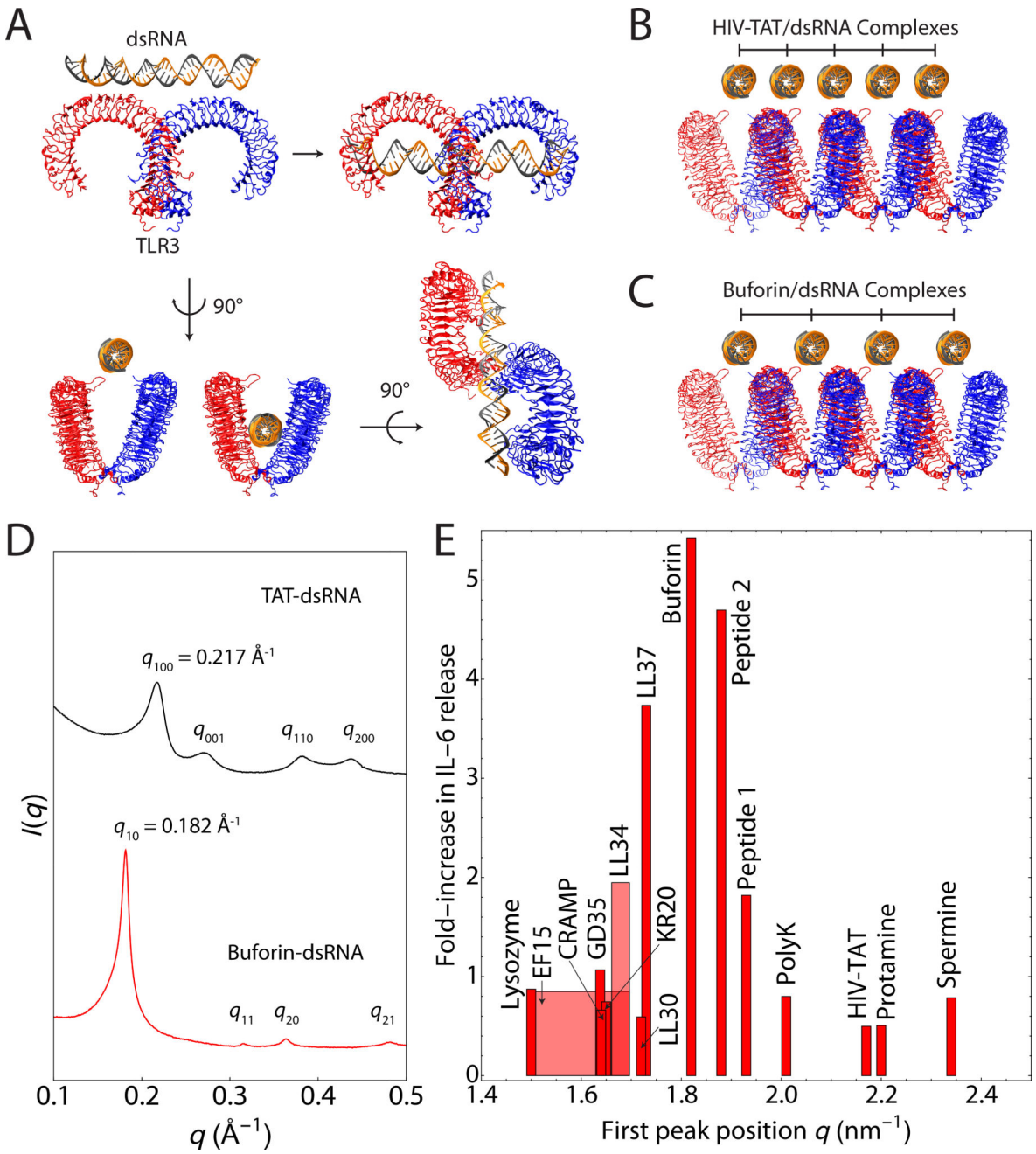

Figure 1. IL-6 production in keratinocytes through TLR3 activation depends on the inter-dsRNA spacing within self-assembled polycation-dsRNA electrostatic complexes

(**A**) Illustration of dsRNA binding to TLR3 from two orthogonal views based on the known crystal structure of mouse TLR3 (PDB ID: 3CIY[26]). (**B**) Smaller geometric spacings between ordered dsRNA columns (such as in HIV-TAT/dsRNA complexes) reduce TLR3 activation because they sterically hinder accessibility of dsRNA to the receptors. (**C**) In contrast, larger geometric spacings between ordered dsRNA columns (such as in buforin-dsRNA complex) optimize electrostatic interactions with TLR3, leading to binding of multiple TLR3s simultaneously and amplification of the immune response. (**D**)

Representative SAXS data from peptide-dsRNA complexes that induce strong IL-6 production (buforin-dsRNA, red), and complexes that do not (TAT-dsRNA, black). The TAT-dsRNA complex forms a 3D hexagonal lattice with a first peak position at q_{100} = 0.217 Å^{-1} and an approximate inter-dsRNA spacing of $a \sim 2.90$ nm. The buforin-dsRNA complex forms a 2D hexagonal lattice with a first peak position at q_{10} = 0.182 Å^{-1} and an inter-dsRNA spacing of $a \sim 3.45$ nm. All higher order reflections are labeled. **(E)** Normalized fold-increase in IL-6 production by NHEK induced by polycation-dsRNA complexes. The immune response correlates strongly with the SAXS measurements of their first diffraction peak positions, which are inversely proportional to the inter-dsRNA spacing. The distance correlation test for statistical independence is R_{dCor} = 0.371 [0.327, 0.492] (95% CI) with P = 0.022 (Figure S1A). The MIC nonlinear correlation was MIC = 0.652 [0.414, 0.894] with $P < 10^{-5}$ (Figure S1B). Inter-dsRNA spacings corresponding to first peak positions q~1.7–1.9 nm^{-1} result in amplified IL-6 production. Wide bars with shading indicate a range of first peak positions for two of the polycation-dsRNA complexes (EF15, LL34) based on SAXS measurements. Narrow bars indicate no significant observable change in first peak positions across stoichiometric ratios.

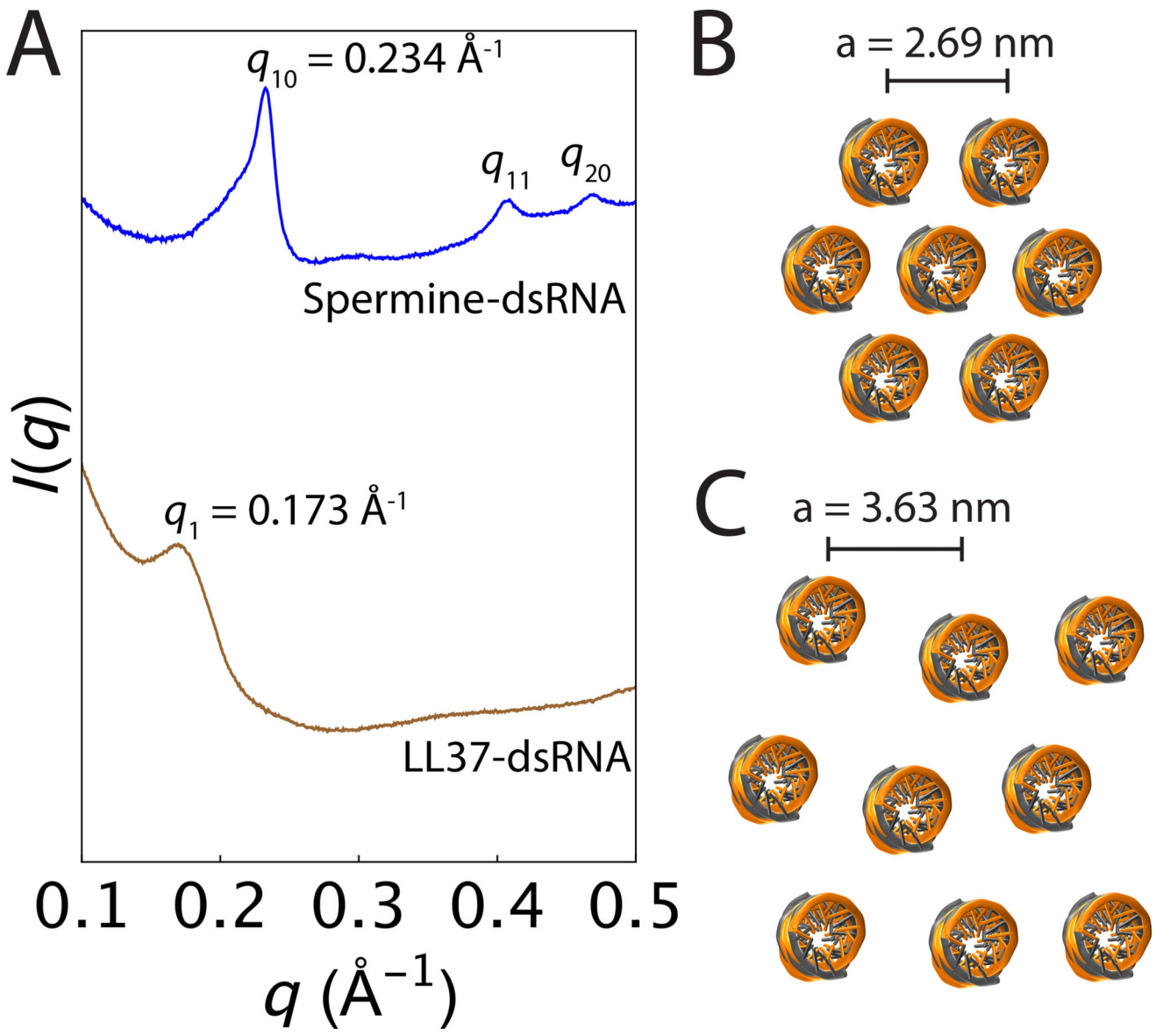

Figure 2. Differences in structure of polycation-dsRNA complexes predict their abilities to amplify cytokine production

Ordered dsRNA columnar complexes have diverse structures with varying inter-dsRNA spacings. The presentation of "open" dsRNA complexes with spacings commensurate with the steric size of TLR3 (a = 3.3–3.7 nm) highly amplify IL-6 production in NHEK, while "closed" dsRNA complexes with spacings smaller than the steric size of TLR3 (d < 3.2 nm) result in reduced TLR3 activation and IL-6 production. (**A**) Representative SAXS data of spermine and LL37-dsRNA complexes. LL37-dsRNA complexes induce ~5× the IL-6 production from NHEK compared to spermine-dsRNA complexes. Spermine-dsRNA complexes (blue) form a 2D hexagonal columnar phase with a first peak position at q_{10} = 0.234 Å^{-1}, corresponding to an inter-dsRNA spacing of a = 2.69 nm (**B**). All higher order reflections of the spermine-dsRNA complex are labeled with their Miller indices. In comparison, the LL37-dsRNA complexes (brown) form a disordered columnar phase with a

first peak position at $q_1 = 0.173$ Å^{-1} and an average inter-dsRNA spacing of $a = 3.63$ nm (**C**). This difference in inter-dsRNA spacing drastically changes the ability of the complex to activate TLR3, as observed in Figure 1E.

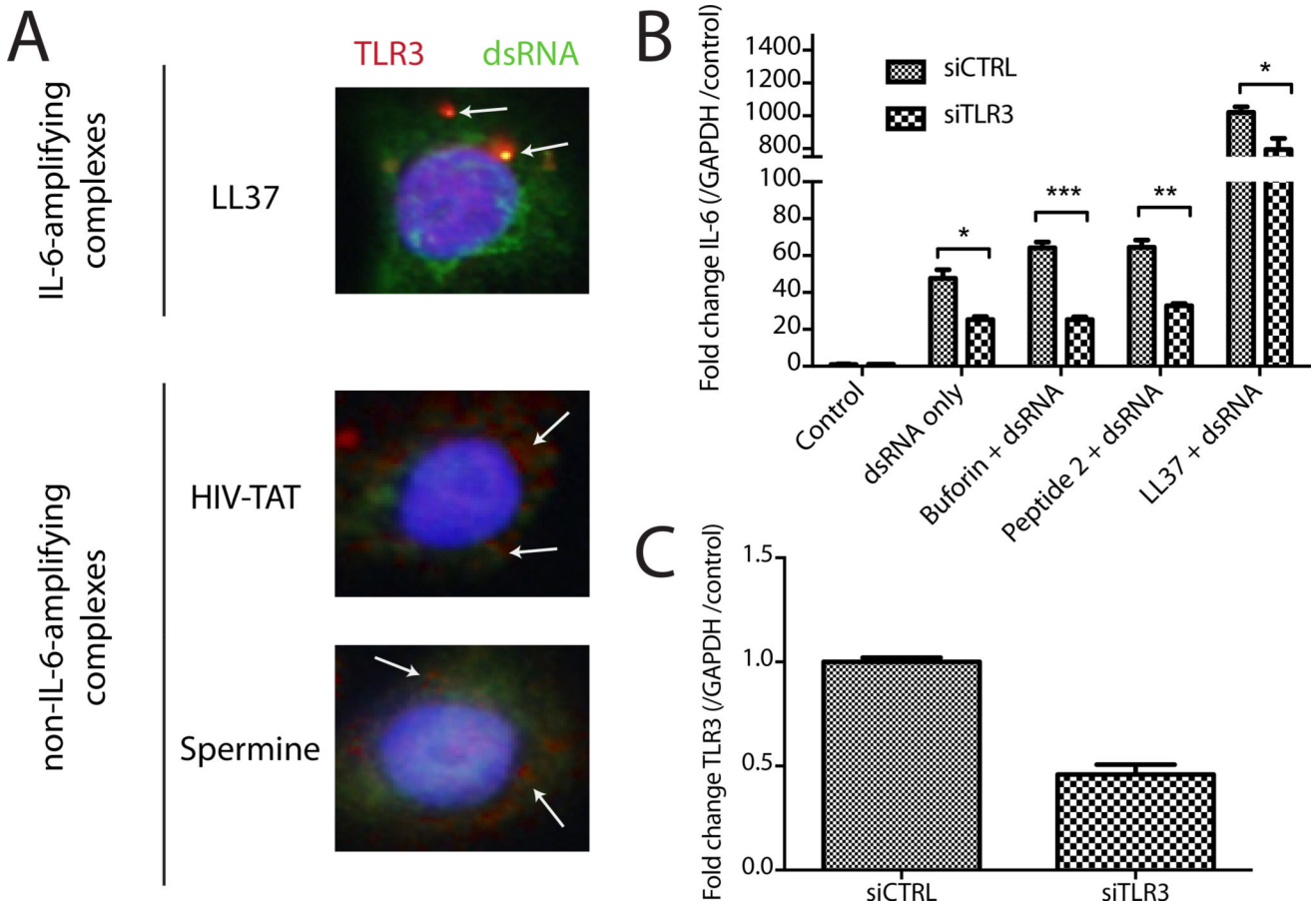

Figure 3. Cytokine-inducing polycation-dsRNA complexes activate NHEK *via* TLR3

NHEK were stimulated for 4 hrs with biotinylated poly(I:C) complexed with either IL-6-amplifying LL37 or non-IL-6-amplifying HIV-TAT and spermine. Cells were fixed in 4% PFA for 10 mins, and then incubated with rabbit anti-TLR3. After washing, AlexaFluor 488-labelled streptavidin was used to visualize poly(I:C), and 576-labeled anti-rabbit secondary antibody was used to visualize TLR3. Cell nuclei were stained with DAPI. Cells were imaged using an Olympus BX41 microscope. **(A)** We observe strong co-localization between TLR3 (red) and polycation-dsRNA complexes (green) within NHEK (white arrows indicate overlap). Both IL-6-amplifying and non-IL-6-amplifying polycation-dsRNA complexes co-localize with TLR3, indicating that endosomal access is a necessary but not sufficient criterion for high levels of cytokine production. (**B**) RTqPCR of IL-6 transcripts during siRNA knockdown of TLR3 confirms that TLR3 activation by strongly-activating polycation-dsRNA complexes are predominantly responsible for IL-6 production. The buforin-poly(I:C), Peptide 2-Poly(I:C), and LL37-poly(I:C) complexes all demonstrate statistically significant reduction in IL-6 production in the presence of siTLR3 compared to control siRNA ($p^* < 0.05$ for dsRNA only, $p^{***} < 0.001$ for buforin-dsRNA, $p^{**} < 0.01$ for Peptide 2-dsRNA, $p^* < 0.05$ for LL37-dsRNA). Data is shown relative to expression of the GAPDH housekeeping gene. (**C**) Data showing successful knockdown of TLR3 in NHEK using siTLR3 ($p < 0.001$). Pairwise two-tailed t-tests were used to analyze siRNA knockdowns in both (**B**) and (**C**) (Error bars show mean ± SEM, n = 3).

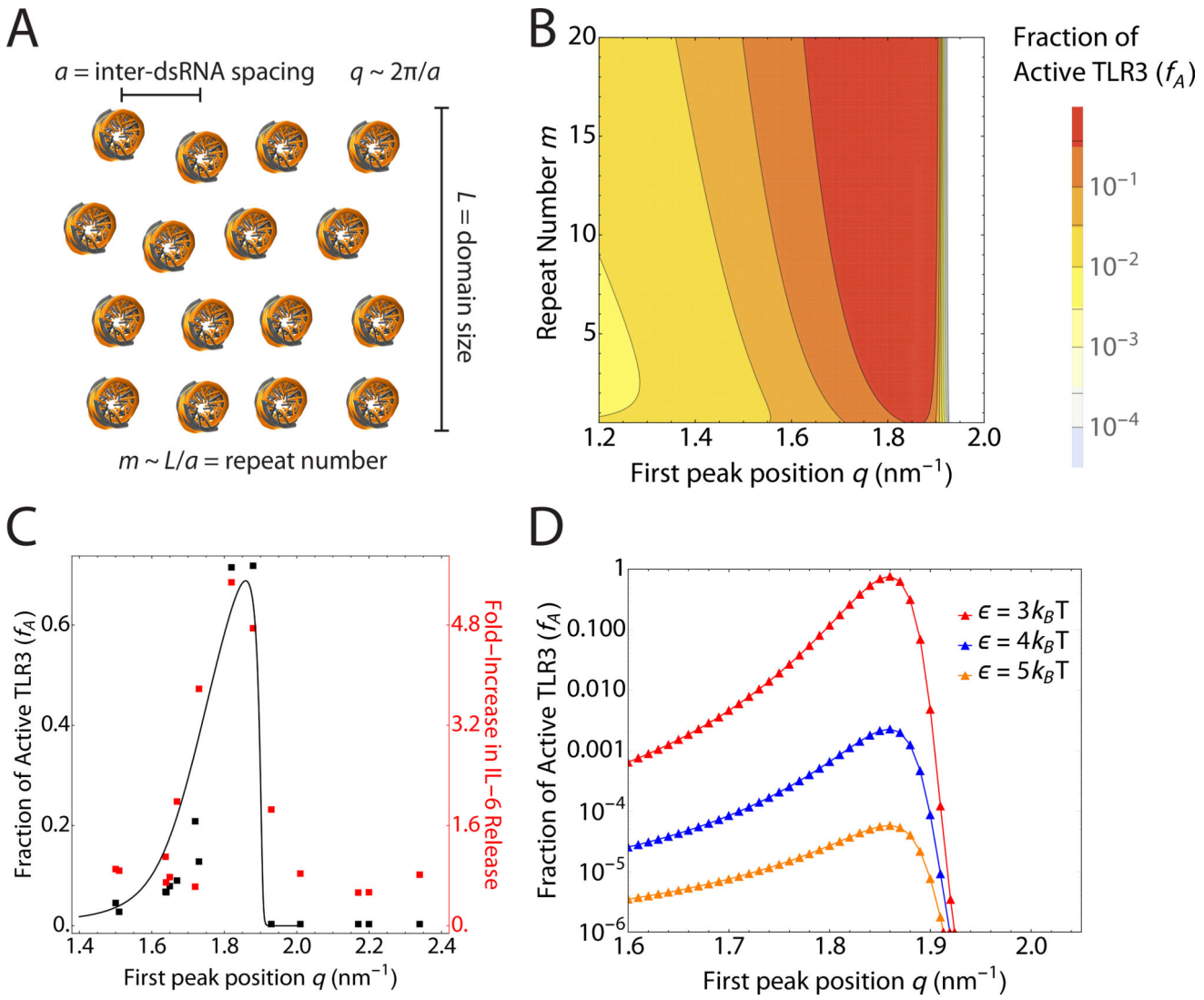

Figure 4. Coarse-grained model of TLR3 binding to RNA bundles exhibits dependence on inter-dsRNA spacing and repeat number in agreement with experimental observations

(**A**) Schematic depicting the crystallinity parameters of an example peptide-dsRNA complex. The inter-dsRNA spacing, first peak position, domain size, and repeat number are defined. (**B**) Contour plot of the fraction of active TLR3 receptors f_A as a function of the repeat number m (*e.g.* number of dsRNA rods per cluster) and the first peak position q, which is inversely proportional to the inter-dsRNA spacing ($a = 2\pi/q$). For this snapshot, the prefactor was chosen as $C^* = l\frac{c_{RNA}}{\rho_{TLR}} = 10^{-2}$, with interaction energy $\epsilon^* = 2\ k_BT$. The TLR3-RNA interaction model was used with the backbone electrostatic interaction magnitude $B = 30\ k_BT$ nm and the steric size of TLR3 $\sigma = 4.4nm$, which is wider than TLR9 due to a larger opening angle. High levels of TLR3 binding and TLR3 activation are denoted in orange, and low levels of binding and TLR3 activation are denoted in yellow to blue. We observe that maximal activation occurs at inter-dsRNA spacings corresponding to first-peak positions $q = 2\pi/a$ between $q \sim 1.7$–1.9 nm^{-1} (~3.3–3.7 nm), but that this region expands as repeat

number increases. Inter-dsRNA spacings that are much smaller than the steric size of TLR3 do not lead to increased activation ($q > 2.0\ \mathrm{nm}^{-1}$) due to steric repulsion between adjacent receptors and dsRNA rods. (**C**) To compare the theoretical prediction of TLR3 activation to the experimental data for the 15 characterized complexes, we calculate the fraction of active TLR3 f_A using the parameters q and m from Table S1 and SI Eqn 3. We find good quantitative agreement between the theoretical prediction of active TLR3 (left vertical axis, black) and measured IL-6 production from NHEK (right vertical axis, red) for experimentally measured q and m (Figure 1E). The vertical axes are rescaled for consistency. To guide the eye, the black line denotes the theoretical curve from SI Eqn. 3 calculated for $m = 6$. (**D**) Grand canonical Monte Carlo simulations of TLR3 binding to crystalline lattices of dsRNA recapitulate features observed in the theoretical model and experimental data. The fraction of active TLR3 receptors (f_A) is plotted against the first peak position q at the cluster size $m = 4$ for interaction energies $\varepsilon^* = 3\ k_B T$, $4\ k_B T$, and $5\ k_B T$. The interaction parameters are the same as above (B).

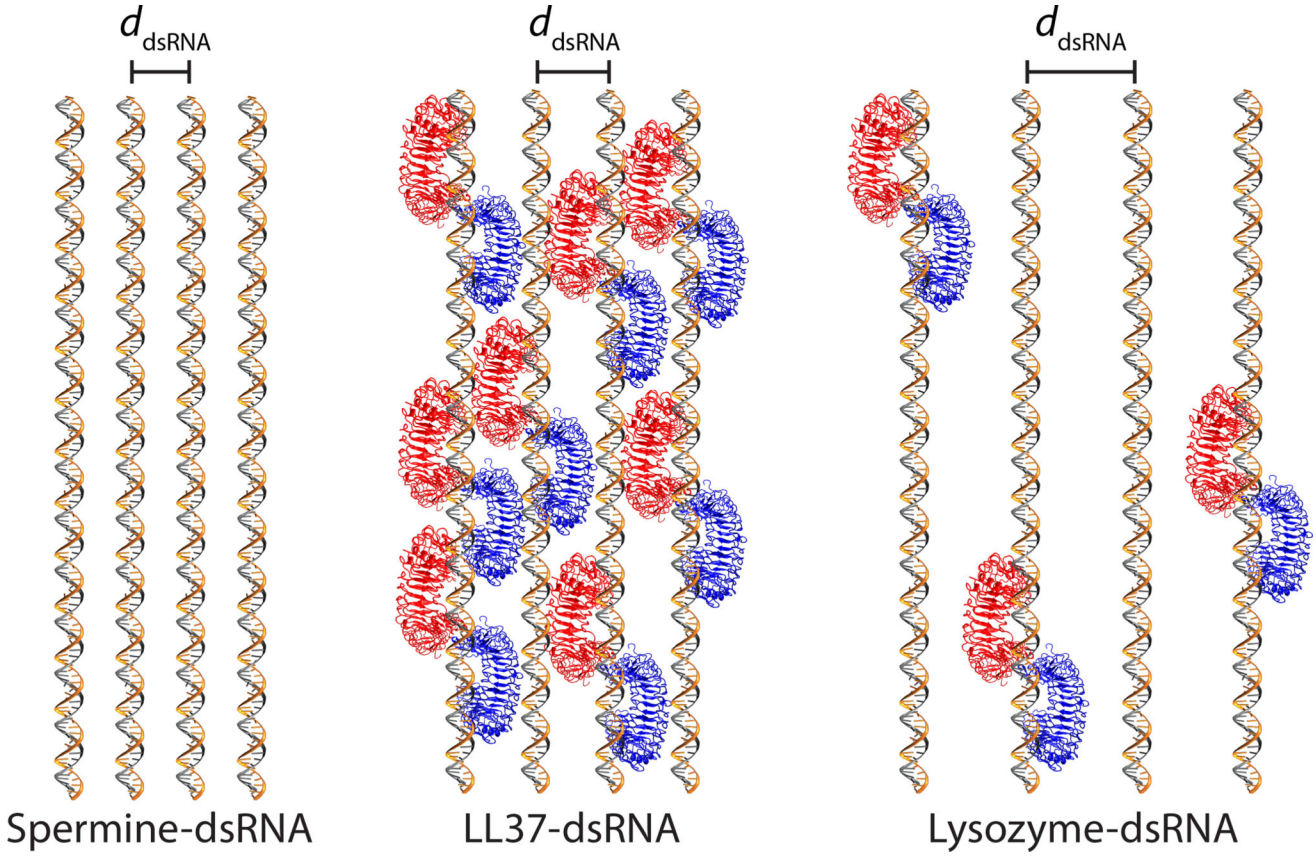

Figure 5. Superselective binding of TLR3 to polycation-dsRNA complexes occurs only at inter-dsRNA spacings commensurate with the steric size of TLR3

This schematic demonstrates the drastic differences in TLR3 binding and activation as the inter-dsRNA spacing is varied from “close-packed” to “open”. This is a top-down view of mobile TLR3 receptors (red and blue) in the endosomal membrane binding to clustered dsRNA ligands (gray). Spermine-dsRNA complexes with tightly packed dsRNA rods does not allow for steric access of TLR3 paddles between rods. LL37-dsRNA complexes have optimal inter-dsRNA spacings well-matched to the width of the TLR3 paddles, which drives TLR3 receptor recruitment and clustering and drastically amplifies immune activation. “Wide-packed” lysozyme-dsRNA complexes can accommodate TLR3 binding and activation, but loss of multivalency between adjacent dsRNA rods due to reduced backbone interactions leads to a lower density of TLR3 binding.